THE JOURNAL OF COMPARATIVE NEUROLOGY 471:11–25 (2004)

Cellular Patterns in the Inner Retina of Adult Zebrafish: Quantitative Analyses and a Computational Model of Their Formation

DAVID A. CAMERON[1]* AND LAUREL H. CARNEY[2]
[1]Department of Neuroscience and Physiology, State University of New York–Upstate Medical University, Syracuse, New York 13210
[2]Department of Bioengineering and Neuroscience and the Institute for Sensory Research, Syracuse University, Syracuse, New York 13244

ABSTRACT

The mechanisms that control cellular pattern formation in the growing vertebrate central nervous system are poorly understood. In an effort to reveal mechanistic rules of cellular pattern formation in the central nervous system, quantitative spatial analysis and computational modeling techniques were applied to cellular patterns in the inner retina of the adult zebrafish. All the analyzed cell types were arrayed in nonrandom patterns tending toward regularity; specifically, they were locally anticlustered. Over relatively large spatial scales, only one cell type exhibited consistent evidence for pattern regularity, suggesting that cellular pattern formation in the inner retina is dominated by local anticlustering mechanisms. Cross-correlation analyses revealed independence between the patterns of different cell types, suggesting that cellular pattern formation may involve multiple, independent, homotypic anticlustering mechanisms. A computational model of cellular pattern formation in the growing zebrafish retina was developed, which featured an inhibitory, homotypic signaling mechanism, arising from differentiated cells, that controlled the spatial profile of cell fate decisions. By adjusting the spatial profile of this decaying-exponential signal, the model provided good estimates of all the cellular patterns that were observed in vivo, as objectively judged by quantitative spatial pattern analyses. The results support the hypothesis that cellular pattern formation in the inner retina of zebrafish is dominated by a set of anticlustering mechanisms that may control events at, or near, the spatiotemporal point of cell fate decision. J. Comp. Neurol. 471:11–25, 2004.

Indexing terms: pattern formation; development; *Danio rerio*; retina

The neural retina of vertebrates has long been recognized as a structure with a high degree of spatial order. Perhaps the most prominent element of the retina's cellular organization is the laminar profile of three nuclear and two plexiform layers (Müller, 1857; Ramón y Cajal, 1893; Polyak, 1941). Although less commonly recognized, the neural retina is also highly organized within its tangential plane. Hannover (1840) described a nonrandom, square-like pattern of photoreceptors across the fish retina, and nonrandom patterns of photoreceptors have subsequently been reported in many species, including teleosts (for reviews, see Engström, 1963; Ali and Anctil, 1976; Stenkamp and Cameron, 2002) and mammals (e.g., Williams, 1988; Wikler and Rakic, 1990). Nonrandom patterns of other retinal cells have also been reported across the vertebrate subphylum (e.g., Hibbard, 1971; Wässle and Riemann, 1978; Podugolnikova, 1985; Kouyama and Marshak, 1997; for reviews, see Cook and Chalupa, 2000; Reese and Galli-Resta, 2002). These nonrandom cellular patterns are believed to be of fundamental importance to the retina's ability to process the visual scene.

*Correspondence to: David A. Cameron, Department of Neuroscience and Physiology, SUNY Upstate Medical University, 750 E. Adams St., Syracuse, NY 13210. E-mail: camerond@upstate.edu

Received 16 May 2003; Revised 15 September 2003; Accepted 24 September 2003

DOI 10.1002/cne.11040

Published online the week of February 2, 2004 in Wiley InterScience (www.interscience.wiley.com).

In contrast to invertebrates, however (notably the *Drosophila* eye; for reviews, see Zipursky and Rubin, 1994; Bonini and Choi, 1995; Kopan and Cagan, 1997), the mechanisms that underlie cellular pattern formation in the vertebrate central nervous system are poorly understood. For example, in the vertebrate retina the identity and spatial profiles of the molecular signals that regulate cellular pattern formation are mostly unknown, the spatial correlations between the patterns of distinct cell types are not entirely established, and the long-range spatial attributes of these cellular patterns have not been fully characterized. To improve our understanding of the structure and assembly of cellular patterns in the central nervous system, the present study applied auto- and cross-correlation spatial analyses, as well as computational modeling techniques, to the investigation of cellular patterns and pattern formation in the inner retina of the zebrafish.

We report that cellular pattern formation in the inner retina of zebrafish seems to be dominated by a set of homotypic anticlustering mechanisms. With the possible exception of PKC-positive bipolar cells, there was little evidence to suggest the operation of spatial organizing mechanisms that operate across long spatial scales. Evidence for independence between cellular patterns was observed, suggesting that homotypic cellular patterns themselves may not provide instructive patterning cues for other cell types.

A computational model of cellular pattern formation during zebrafish retinal growth was developed, which featured a relatively simple, inhibitory mechanism for controlling cell fate decisions during retinal growth. This model provided good estimates of all the empirically observed cellular patterns, regardless of a cell's type or intrinsic density. These results suggested that cellular pattern formation in the inner retina of zebrafish may be dominated by a set of homotypic, anticlustering signaling mechanisms that operate over relatively short spatial distances and that may control pattern formation at, or proximal to, the spatiotemporal point of cell fate decision.

MATERIALS AND METHODS

Tissue processing and pattern analyses

All experiments utilizing zebrafish were approved by the Committee for the Humane Use of Animals, SUNY Upstate Medical University. For all experiments retinas were isolated from light-adapted adult zebrafish (*Danio rerio*) that were approximately 2.5 cm in standard length. The methodology for selectively labeling cells in zebrafish retinal whole mounts has been described previously (Cameron and Carney, 2000). Briefly, retinas were isolated from euthanized animals (exposure to 0.2% tricaine followed by exsanguination), fixed (4% paraformaldehyde/0.25% picric acid/0.1 M PO_4 buffer; pH 7.2), and processed for indirect fluorescence immunohistochemistry using two of the following primary antibodies: anti-PKC (rabbit; Chemicon, Temecula, CA), anti-serotonin (rat; anti-5-HT; Chemicon), anti-somatostatin (rabbit; DiaSorin, Stillwater, MN); anti-substance P (rabbit; DiaSorin), or anti-tyrosine hydroxylase (mouse anti-TH; Chemicon). Primary antibody labeling was visualized via secondary antibody conjugated with a fluorophore (fluorescein isothiocyanate [FITC]- or tetramethylrhodamine isothiocyanate [TRITC]-conjugated; Sigma, St. Louis, MO). For double-labeled retinas the antibodies were selected so that different fluorophores were associated with the two primary antibodies (e.g., rat anti-5-HT and mouse anti-TH). Epifluorescence observation of reacted whole mounts was performed with a Zeiss Axioskop microscope, and digital images were collected (e.g., Fig. 6; Metamorph, Universal Imaging, Downingtown, PA).

For each labeled whole mount, circular fields were selected for analysis (Cameron and Easter, 1993). The sampled fields were digitized, and each cell was assigned a coordinate position within two-dimensional space (1-μm resolution). For each sampled field the pattern of labeled cells was quantitatively analyzed using nearest neighbor distance (NND), density recovery profile (DRP), and quadrat analyses. The NND and DRP analyses were performed in either auto- or cross-correlation mode, the former involving homotypic cells and the latter involving cells of two different types. For example, in an auto-NND (aNND) analysis, the distance to the nearest homotypic cell is determined, whereas in the cross-NND (cNND) analysis, the distance to the nearest heterotypic cell is determined. Details of the attributes, application, and statistical testing of these spatial analysis techniques have been provided previously (e.g., NND: Cook, 1996; Cameron and Carney, 2000; DRP: Rodieck, 1991; Cameron and Carney, 2000; Stenkamp et al., 2001; quadrat analysis: Stenkamp et al., 2001). Quadrat analysis, which provides a profile of a pattern's long-range characteristic (regularity, aggregation, or neither regular nor aggregated), involves sequentially parceling a sampled region into grids of dimension ($N \times N$), with N ranging from 1 to 10. For each grid, a dispersion "index" was derived, which was referred to the expected values for a pattern that was either regular, aggregated (clumpy), or neither (see p. 62 of Grieg-Smith, 1964). As in a previous study (Stenkamp et al., 2001), statistical significance ($P < 0.05$) was observed for all analyzed cellular patterns, for $N \geq 9$ (i.e., abscissas of Fig. 7).

Computational modeling

A computational model of cellular pattern formation in the inner retina of zebrafish was developed within the MatLab environment (Math Works, Cambridge, MA). The foundation of this model is the hypothesis that during retinal growth in the zebrafish, cellular pattern formation is regulated, at least in part, by signals that control the spatial profile of cell fate decisions at the circumferential germinal zone (CGZ).

The model consists of two "cellular" components that mimic the cellular organization of the teleost retina: an annular band of precursor cells (analogous to the CGZ,

Abbreviations

aDRP	autocorrelation density recovery profile
aNND	autocorrelation nearest neighbor distance
cDRP	cross-correlation density recovery profile
CGZ	circumferential germinal zone
cNND	cross-correlation nearest neighbor distance
DRP	density recovery profile
5-HT	serotonin
NND	nearest neighbor distance
PKC	protein kinase C
Som	somatostatin
Sub P	substance P
TH	tyrosine hydroxylase

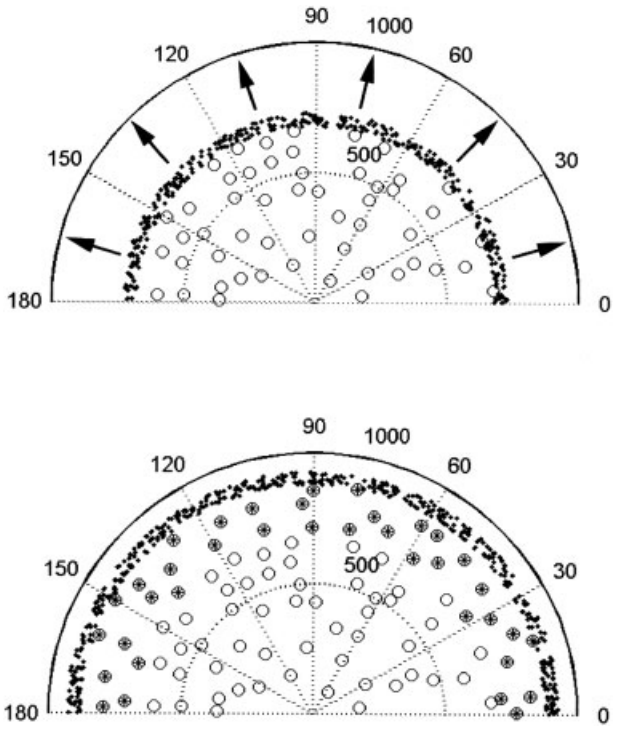

Fig. 1. Schematic of retinal growth in the computational model. The model starts (top) with an empirically derived seed of a two-dimensional cellular pattern, illustrated by the open circles (in this case, TH-positive cells) juxtaposed to an encircling band of undifferentiated cells (i.e., a model CGZ), illustrated by the filled symbols (symbols are not to scale). For simplicity, only a hemicircle of retina is illustrated. The outward-going, spoke-like dotted lines indicate degrees, and the annular dotted lines (500 and 1,000) indicate radial distance in micrometers. Like the situation in vivo, the model retina "grows" outward (arrows) by adding new cells to the retinal margin (crossed circles, bottom). These new cells are derived directly from CGZ cells that differentiate into that particular cell type, without any subsequent lateral movement. New CGZ cells are added to the periphery of the CGZ in a random two-dimensional pattern, and the process continues. The signaling mechanism(s) that controls whether or not a particular CGZ cell differentiates is presented in Materials and Methods.

from whence new cells are generated and appositionally added to the retina throughout life; for review, see Powers and Raymond, 1990), juxtaposed to a central, two-dimensional field of differentiated cells (Fig. 1). The latter serves as a "seed" of differentiated cells and is derived directly from the empirically observed cellular patterns of this report.

The dynamic growth aspect of the model is as follows. Along an arc of the precursor cells, individual cells either will, or will not, become the same cell type as in the central seed. (For computational simplicity, the current model was restricted to the generation of a single type of cell.) As time progresses the band of precursors grows outward, away from the seed, leaving a two-dimensional distribution of newly differentiated cells in its wake. These precursor cells are arrayed in a random spatial pattern—which in terms of this study represents a worst-case, but analytically well-defined, scenario—but any two-dimensional pattern can be imposed. The rate of outward vectorial growth is a model variable, and we note that the amount of retinal area added per unit time in vivo may be a constant (Cameron, 1995). To mimic the geometry of actual retinal growth, the model operates within polar coordinates.

Independent model parameters were estimated from histological observations of adult zebrafish retina. These parameters were the density and distribution of undifferentiated precursor cells (the former was estimated from inspection of cryosections through adult zebrafish retinas to be approximately 5,100 cells/mm^2, and values above this did not affect the results), and the width of the band of undifferentiated precursors (set at 50 μm). Simulations indicated that these are critical parameters in the model: large-scale alterations to these anatomy-based parameters could hinder the model's ability to recapitulate cellular patterns (e.g., CGZ widths of greater than 200 μm, or densities of precursor cells that were too low.). Because such alterations are poor representations of the retinal organization in situ, they are not discussed in detail in this report.

In the current model the signal that controls cell fate decision is derived directly from differentiated cells and functions to *inhibit* the precursor cells' acquisition of the homotypic cell fate (Fig. 2). The spatial profile of the signal is a first-order decaying exponential that originates from each seed cell (with amplitude at the source defined as +1.0). The mean and variance of the exponential function's space constant (λ_i) are independent variables, set prior to each simulation; for the simulations in this report, the standard deviation was set to 10% of the mean. Variation in the spatial profile of the signaling mechanism was included in the model because of the recognized complexity (nonlinearity) of the spatial profiles of signaling mechanisms in situ (Strigini and Cohen, 1999; Vincent and Dubois, 2002). Lateral movements of differentiated cells (e.g., Diaz-Araya and Provis, 1992; Robinson and Hendrickson, 1995; Reese et al., 1995, 1999; Eglen et al., 2000; Eglen and Willshaw, 2002) are allowed by the model but were not invoked in the current study because they did not significantly affect the outcome (see Results).

The model operates in the following manner. Along the band of precursor cells in the CGZ (limited to an arc of 120° to reduce computational time), a cell within 50 μm of a differentiated cell is randomly selected. The summed amplitude of the inhibitory signal, which emanates from all the differentiated cells in the sample, is then calculated for that location (Fig. 2). If the signal amplitude is above some threshold value (an independent variable that is set relative to the signal amplitude at an individual source cell), the precursor cell is "inhibited" and remains undifferentiated. Another precursor cell in the CGZ is then randomly selected, and the process is repeated. If the signal amplitude is *below* the preset threshold value, the precursor cell acquires the cell fate of the seed and immediately begins to emit the inhibitory signal with space constant of λ_i at the preset mean and standard deviation. Note that for all subsequent evaluations, the inhibitory signal arising from this new "differentiated" cell contributes to the overall spatial profile of the inhibitory signal across two-dimensional space. The process of randomly selecting precursor cells within 50 μm of the seed is repeated until all cells have been sampled, at which point a new set of randomly positioned CGZ cells is appositionally added to the periphery—that is, the model retina is driven to grow outward—and the process of precursor cell evaluation is repeated. For each simulation, the number of

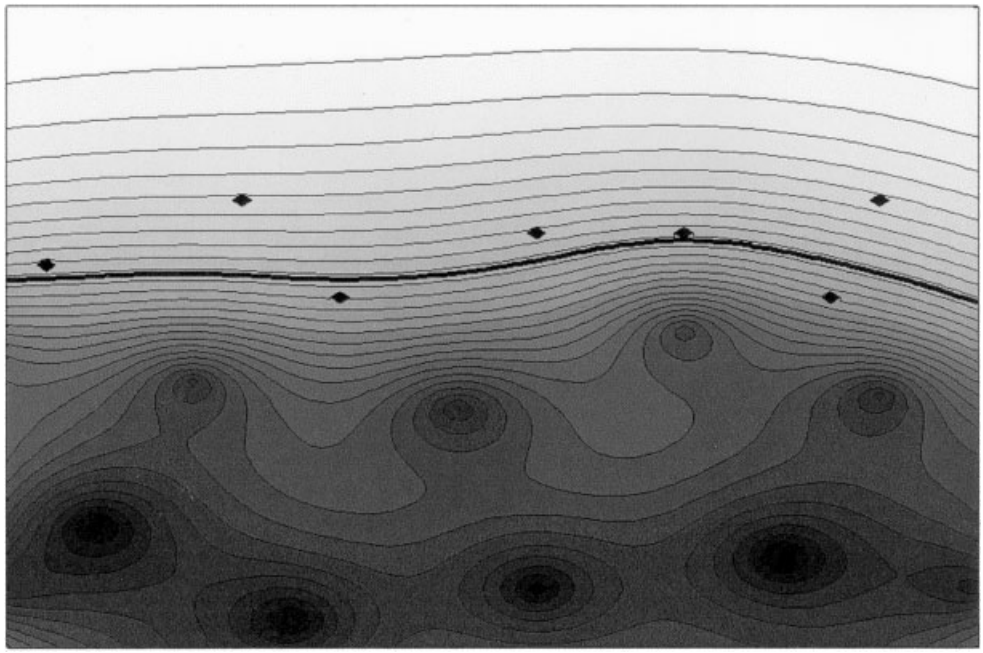

Fig. 2. Schematic of the signaling mechanism used in the computational model of cellular pattern formation. Each differentiated cell of a particular type is the source of a signal (dark color) that decays exponentially over distance with some space constant (λ_i; eight differentiated cells are shown, which appear as the darkest profiles in the bottom half of the figure). This signal, when present at suprathreshold levels, inhibits precursor cells within the CGZ from acquiring the fate of the source cells. (Seven precursor cells are shown, indicated by black diamonds.) An arbitrarily chosen threshold level is illustrated as the thick contour line running from left to right on the figure. The precursor cells below this line (n = 2 in this example) are inhibited, whereas those above the line, given the current distribution of the inhibitory signal, could acquire the fate of the source cells. By selecting the appropriate values of λ_i and threshold, the model generated good estimates of all the empirically observed cellular patterns (see Results and Figs. 9 and 10).

CGZ additions (i.e., the absolute radial distance of retinal growth) is set.

The current model has several features that distinguish it from earlier models of cellular pattern formation in the teleost retina (e.g., Takesue et al., 1998; Tohya et al., 1999). These features include operating within polar coordinates to mimic the geometry of actual retinal growth (as opposed to the rectilinear coordinates of earlier models), the lack of a pre-existing nonrandom lattice of compartments within which differentiated cells are forced to reside, and the allowance of signaling mechanisms that extend beyond that of direct soma-to-soma contact (e.g., a diffusible signaling mechanism, or a dendrite-like cell contact mechanism). The latter attribute of the model is particularly important because, for example, diffusible agents have been implicated in vertebrate retinal development, including zebrafish (e.g., retinoic acid, Hyatt et al., 1996; *sonic hedgehog*, Stenkamp et al., 2000; Neumann and Nuesslein-Volhard, 2000).

RESULTS

The labeled cells in this report are designated as belonging to a certain cell type, with the word "type" signifying only the positive immunohistochemical labeling. Five different inner retinal cell types were analyzed for this study, and all labels were non-overlapping. The somata of all these cell types were located within the inner nuclear layer. Based on earlier investigations of fish retina (Marshak et al., 1984; Yazulla et al., 1985; Dowling, 1987; Yazulla and Zucker, 1988; Suzuki and Kaneko, 1990; Cameron and Carney, 2000), the cells were identified as subsets of the amacrine (5-HT-, somatostatin-, and substance P-positive), interplexiform (TH-positive), and bipolar (PKC-positive) cell classes.

Fig. 3. Representative cellular patterns and NND and DRP analyses. **Top row:** Examples of cellular patterns from double-labeled zebrafish retinas. The indicated cell types are immunopositive for antibodies against tyrosine hydroxylase (TH), somatostatin (Som), or serotonin (5-HT). **Second row:** Nearest neighbor distance (NND) results for the patterns illustrated in the top row. For each cell type the plots indicate the fraction of the total number of cells within that type that have a particular NND value. Autocorrelation NND results are indicated by the solid and dashed lines; cross-correlation NND results are indicated by the solid and open bars, with the "direction" of analysis indicated in the key. **Third row:** The autocorrelation density recovery profile (aDRP) results of the same patterns, with the solid and open bars assigned to the indicated cell types. The horizontal solid line indicates the overall density of the cell type assigned to the white bars, and the horizontal dashed line indicates the overall density of the cell type assigned to the solid bars. In DRP analysis, each analyzed cell in a pattern was assigned to abscissa value 0, and the "recovered" density of like-type cells was plotted as a function of annular distance away from each analyzed cell (as in Rodieck, 1991). **Bottom row:** The cross-correlation DRP (cDRP) results of the same patterns. The solid and open bars correspond to the indicated "direction" of analysis; for example, TH > Som denotes that TH-positive cells were the starting points of analysis, and the target cells were somatostatin-positive. The solid and dashed horizontal lines in the cDRP plots thus correspond to the density of the same target cell type as in the corresponding aDRP plot.

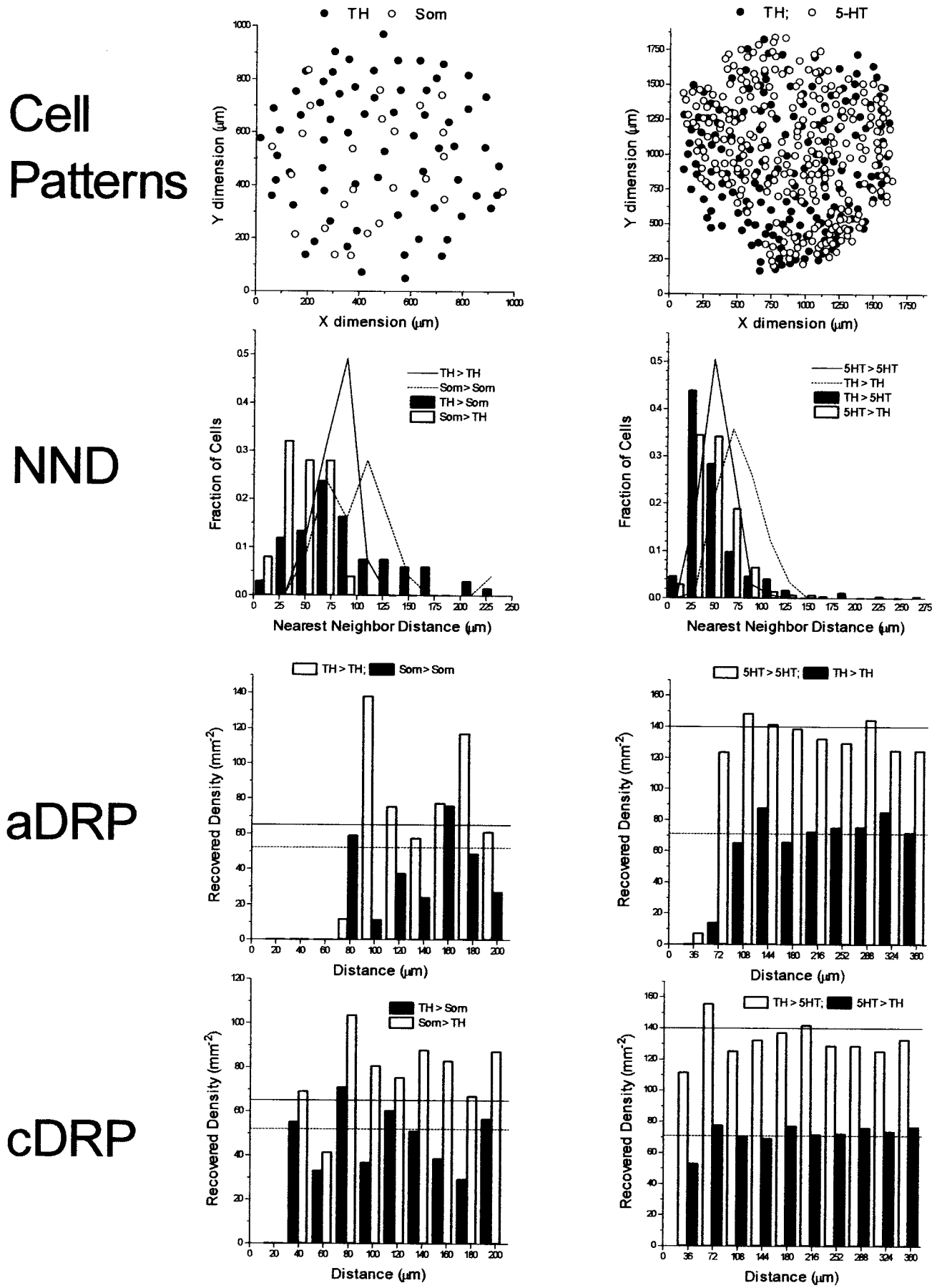
Cell Patterns
NND
aDRP
cDRP
TH
Som
TH;
5-HT
Y dimension (μm)
X dimension (μm)
Fraction of Cells
Nearest Neighbor Distance (μm)
TH > TH
Som > Som
TH > Som
Som > TH
5HT > 5HT
TH > TH
TH > 5HT
5HT > TH
Recovered Density (mm-2)
Distance (μm)
TH > TH; Som > Som
5HT > 5HT; TH > TH
TH > Som
Som > TH
TH > 5HT; 5HT > TH

Figure 3

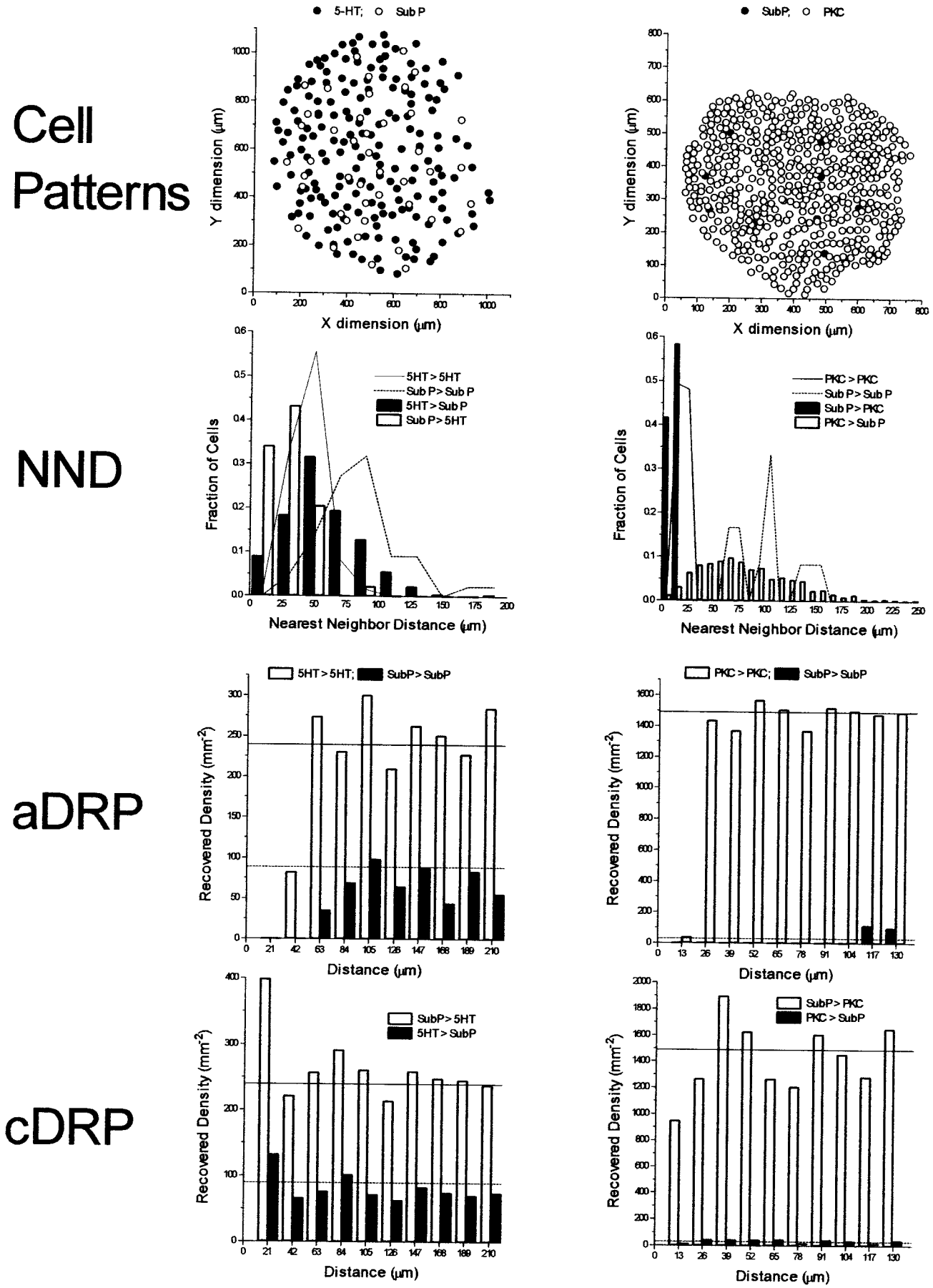

Fig. 4. Representative cellular patterns and NND and DRP analyses. The layout and attributes of the figure are identical to those of Figure 3. In this case, the displayed and analyzed cell types are immunopositive for antibodies against 5-HT, Sub P, and PKC. For abbreviations, see list.

Autocorrelation analyses of cellular patterns

Representative examples of eight cellular patterns from four retinas are presented along the top row of Figures 3 and 4. The aNND (autocorrelation NND) distribution for each of the displayed examples is provided immediately below each pattern (solid lines, second row of Figs. 3 and 4). The NND distribution for a random set of points would follow a Rayleigh distribution (Wässle and Riemann, 1978), and the normal distribution of the aNND data suggested that the patterns were therefore not random. The aNND data were always significantly different ($P < 0.05$, independent t-test) from the NND derived from simulated random patterns that were "matched" to the data by having the same number of non-overlapping cells within the same two-dimensional area. This statistical difference was confirmed by the conformity ratio analysis of Cook (1996): each cell type was arrayed in a two-dimensional pattern that was significantly different (at $P < 0.05$) from the value expected for a random distribution (cf. open symbols and horizontal line of Fig. 5A; Table 1).

For each cell type the effective radius values derived from the aDRP analysis revealed that anticlustering was a dominant characteristic of the patterns (open symbols of Fig. 5B; Table 1), that is, for each soma of a given cell type the surrounding two-dimensional space consisted of a relatively large area that was free of somata of homotypic cells. These exclusion zones—graphically evident as an absence of "recovered" density at low abscissa values in the aDRP plots of Figures 3 and 4 (third row)—were on the order of 3–10 times larger than the diameters of individual somata (Cameron and Carney, 2000; cf. the effective radius values of Table 1 with the somata pictured in Fig. 6). This result indicated that the anticlustering phenomena could arise from signaling mechanisms with spatial profiles that extend beyond that mediated by direct soma-to-soma contact, e.g., signals that are diffusible or are delivered via cellular projections such as dendrites. Furthermore, because the cellular patterns at the peripheral retina (from whence new retinal cells are generated and appositionally added to the teleost retina throughout life) and more central regions are similar (Fig. 6), it was concluded that the observed two-dimensional patterns are established proximal to the point of cellular differentiation, with minimal subsequent modification by "secondary" patterning mechanisms.

Quadrat analysis provided a statistical evaluation of the long-range pattern characteristics of each cell type, in which the long-range profile of a two-dimensional pattern was judged to be either regular, aggregated (clumped), or neither regular nor clumped (e.g., random; David and Moore, 1954; Ripley, 1981; Stenkamp et al., 2001). For each analyzed pattern, the statistical significance of each dispersion "index" value was determined (see Materials and Methods). In approximately 70% of the analyzed patterns (16/23, Table 1), quadrat analysis revealed no statistically significant evidence for a nonrandom pattern characteristic, either regularity or aggregation ($P < 0.05$, χ^2 distribution; Fig. 7 and Table 1), rather, most patterns exhibited long-range profiles that were indistinguishable from those expected for a randomly distributed set of points (i.e., most functions fall within the gray fields of Fig. 7). These results indicated that the nonrandom mechanisms that regulate cellular pattern formation over rel-

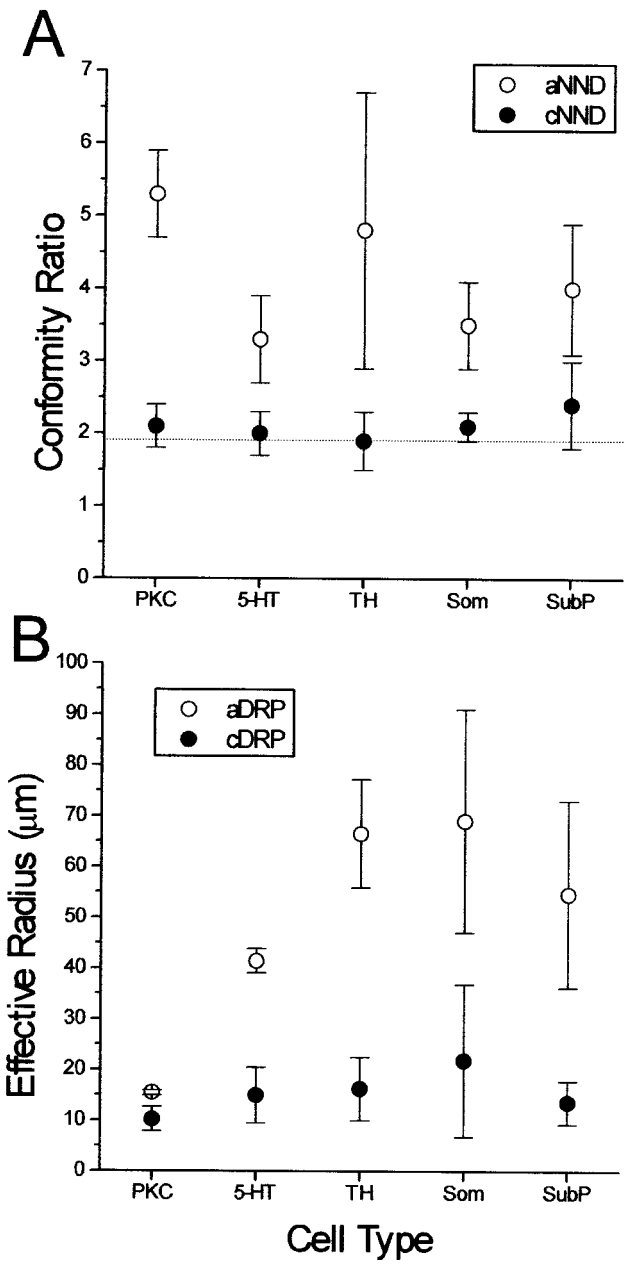

Fig. 5. Summary of NND and DRP analyses. **A:** Conformity ratios (mean ± SD) derived from aNND and cNND analyses (conformity ratios are [mean/SD] of each NND), pooled for each cell type and cell-type pairing. For the latter, the denoted cell type is the "target" of the cNND analysis. Autocorrelation analyses for each cell type (open symbols) had pooled conformity ratios that were significantly different (see Table 1) from that expected for a random distribution of points (approximately 1.9, solid line; Cook, 1996). In contrast, analyses of distances between two cell types had pooled conformity ratios that were not significantly different from that expected for random distributions (see Table 2). **B:** The pooled values of effective radius (mean ± SD; Rodieck, 1991) derived from aDRP and cDRP analysis of each cell type or cell-type pairing, as in A. In the aDRP conditions (open symbols), each cellular pattern was characterized by a relative large area encircling each soma that was devoid of homotypic somata. This result was graphically evident as near-zero "recovered" density at low values along the abscissa of the aDRP plots of Figures 3 and 4 (see also Table 1). In contrast, for each target cell type the effective radius values in the cDRP conditions (solid symbols) were always smaller, indicating a comparative lack of cellular exclusion between the somata of different cell types. For abbreviations, see list.

TABLE 1. Autocorrelation Spatial Analysis Results for Cells in the Inner Retina of Adult Zebrafish[1]

Cell type	Nearest neighbor (μm; mean ± SD, n)	Conformity ratio[2] (mean/SD of NND)	Effective radius (μm; from aDRP)	Quadrat result[3]
PKC-positive	18.7 ± 3.5 (63)	5.3	14.9	Regular
	19.6 ± 4.2 (522)	4.7	15.8	Regular
	13.3 ± 2.3 (281)	5.8	11.5	Regular
5-HT–positive	53.3 ± 15.6 (275)	3.4	40.6	Regular
	45.7 ± 12.9 (46)	3.5	39.5	Random
	44.9 ± 13.3 (180)	3.4	36.5	Random
	42.2 ± 11.5 (49)	3.7	44.1	Regular
	46.0 ± 19.5 (39)	2.4	32.3	Random
Som-positive	101.6 ± 37.8 (25)	2.7	58.8	Random
	87.6 ± 18.0 (16)	*4.9*	82.7	Random
	78.8 ± 22.4 (18)	3.5	70.9	Random
	73.2 ± 14.6 (24)	5.0	56.7	Random
	67.7 ± 8.8 (18)	7.7	63.3	Random
Sub P-positive	102.7 ± 28.3 (12)	*3.6*	103.6	Random
	81.2 ± 25.9 (14)	*3.1*	45.9	Random
	83.1 ± 27.6 (10)	*3.0*	54.9	Random
	109.8 ± 24.4 (10)	*4.5*	69.2	Random
	90.2 ± 26.6 (11)	*3.4*	71.2	Random
TH-positive	78.0 ± 21.4 (173)	3.6	69.4	Random
	53.5 ± 19.5 (8)	*2.7*	29.5	Random
	79.1 ± 15.3 (67)	5.2	75.2	Random
	61.0 ± 14.8 (29)	4.1	53.4	Regular
	58.8 ± 13.2 (31)	4.5	45.3	Regular

[1]For abbreviations, see list.
[2]Italicized conformity ratio values, because of low sample size, cannot be judged as being different from a random distribution (Cook, 1996).
[3]The term "random" indicates a pattern that is neither aggregated nor regular. Pattern type and statistical significance of the analysis were determined as previously described (Stenkamp et al., 2001).

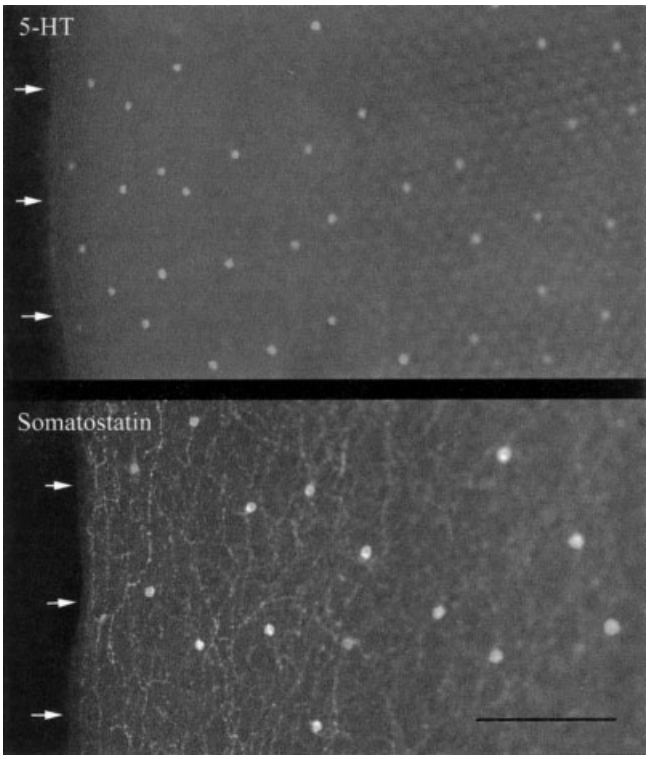

Fig. 6. Evidence for the establishment of inner retinal cell patterns proximal to the point of cellular differentiation. For serotonin (5-HT)-positive cells (**top**) and somatostatin-positive cells (**bottom**), there is little difference in the two-dimensional patterns of cells in central (to the right of each panel) or peripheral retina, right up to the retinal margin (white arrows). Similar observations were made for each of the other cell types analyzed in this report. These pattern characteristics suggested that the observed two-dimensional patterns are established near the point of cell fate decision, with minimal subsequent modification. Scale bar = 100 μm.

atively short distances—inferred from both the aNND and aDRP analysesdo not typically manifest any significant nonrandom pattern characteristics over relatively long spatial scales. Additionally, although such mechanisms could not be formally ruled out, the operation of long-range spatial organizing mechanisms during pattern formation was not evident.

An exception to this general rule was consistently observed. PKC-positive cells, likely to be ON-type bipolar cells (Suzuki and Kaneko, 1990), were always arrayed in patterns that were regular over long spatial distances (i.e., the quadrat analysis functions always fell below the gray field in Fig. 7). It was thus not possible to rule out the possibility that long-range signaling mechanisms control cellular pattern formation for this cell type, although the requirement of such a mechanism is not formally required for any regular pattern. The quadrat analysis profiles of the PKC-positive bipolar cells were reminiscent of those determined for the cone photoreceptor patterns of normal goldfish retina (Stenkamp et al., 2001).

Cross-correlation analyses of cellular patterns

Visual inspection revealed no overt spatial correlations between the patterns of different cell types (top row of Figs. 3 and 4). This qualitative observation was supported by objective, quantitative analyses. The cNND (cross-correlation NND) distributions were consistently shifted to lower values in the distance dimension than the aNND distributions (cf. histogram and line graphs of the NND plots, second row of Figs. 3 and 4), implying a decrease in the size of the cellular exclusion zones. Conformity ratio analysis (Cook, 1996) of the cNND distributions revealed values that were significantly lower than those for the aNND condition ($P < 0.03$, independent t-test; Fig. 5A). Conformity ratio analysis of the cNND pairings also revealed that greater than 60% of the pairings were arrayed in patterns that were statistically independent of one another ($P < 0.05$; values denoted with asterisks in Table 2); for example, for each cell the somata of a heterotypic cell were not excluded from the local area.Most of the remaining cell pairings, which had sample sizes too low for statistical evaluation (italicized values in Table 2), had conformity ratios that were consistent with independence between the cellular patterns (cf. solid symbols and dotted line of Fig. 5A; Cook, 1996).

The inference of independence between the patterns of heterotypic cells was supported by the cDRP analysis (bottom row of Figs. 3 and 4). The effective radius values in the cDRP condition were consistently lower than those observed for the aDRP condition (Fig. 5B; Tables 1, 2). These differences were statistically significant for all analyzed cell-type pairs ($P < 0.004$; independent t-test). Relative to the aDRP condition, the cDRP plots consistently revealed a lower distance along the abscissa at which the heterotypic cell's density (as opposed to the homotypic cell's density) was recovered (cf. the exclusion zones of the corresponding aDRP and cDRP plots of Figs. 3 and 4). Because both the conformity ratio and effective radius

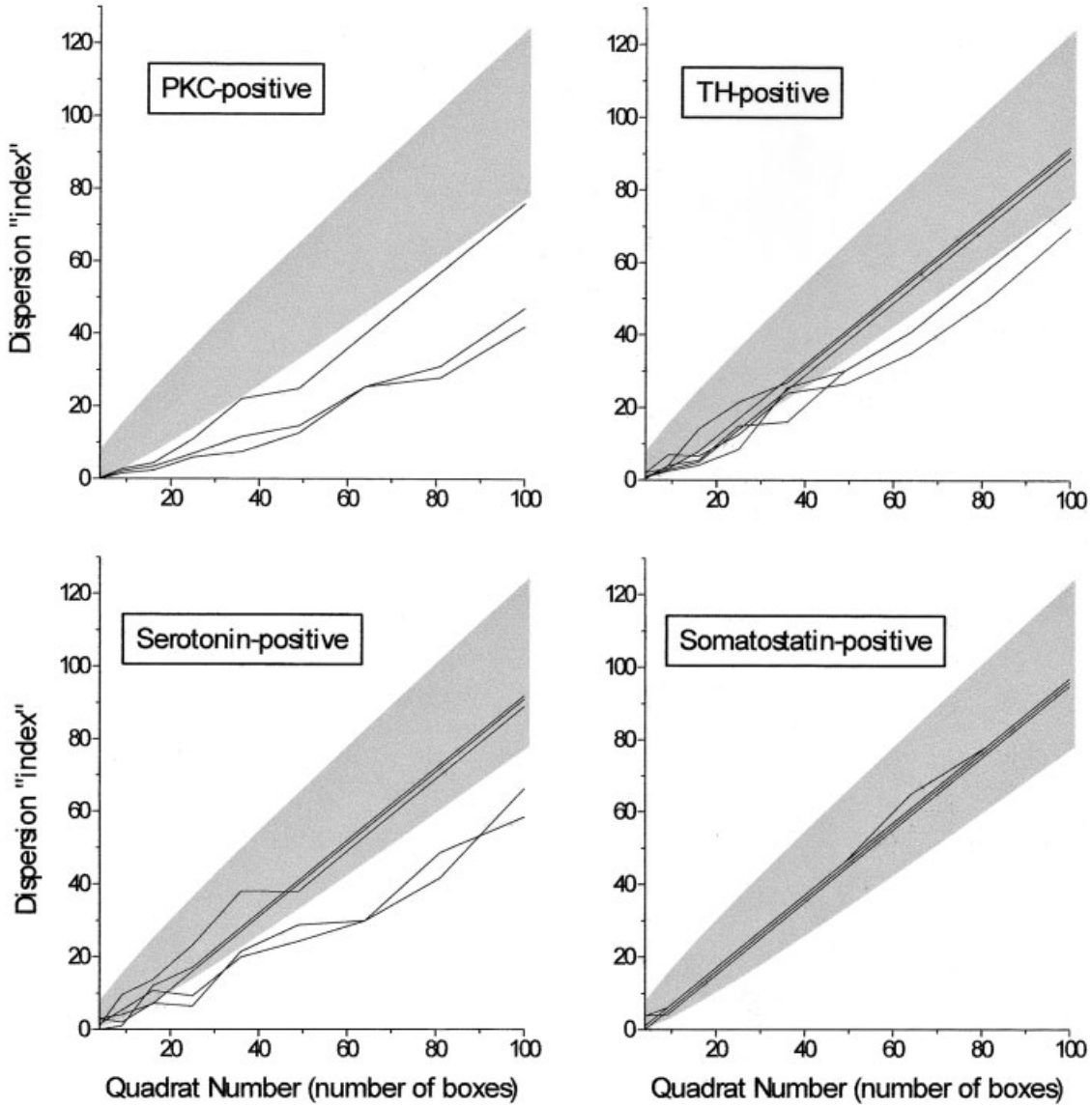

Fig. 7. Summary of quadrat analyses. In each panel the quadrat number (i.e., the total number of square parcellations superimposed upon each sampled region; (N × N) from Materials and Methods) is plotted as a function of the dispersion "index" (actually a statistic) derived for each analyzed pattern of that particular cell type, as in Stenkamp et al. (2001). Statistical significance was observed for all quadrat numbers ≥ 9 (Grieg-Smith, 1964). In each panel, the functions for individual cellular patterns are indicated by the solid lines, and the gray field is that region within which dispersion index values for nonregular or nonaggregated (e.g., random) patterns would be expected. For PKC-positive cells, every analyzed pattern was statistically regular (i.e., the functions were all below the grey field). For TH- and 5-TH–positive cells, most patterns were nonregular and nonaggregated, that is, most functions were completely within the gray field. For somatostatin-positive cells (and substance P-positive cells; data not shown) all the analyzed patterns were nonregular and nonaggregated. These results suggested that with the exception of PKC-positive cells, over large spatial extents most cellular patterns were not statistically different from random patterns. For abbreviations, see list.

values in the cross-correlation analyses were independent of the direction of cell-to-cell analysis (i.e., measuring from cell type "A" to cell type "B," and vice versa), it was concluded that differences in cellular densities did not introduce artifactual, positive correlations between cell patterns (Table 2). The quantitative, cross-correlation analyses thus supported the hypothesis that the different inner retinal cell types analyzed in this study were arrayed in spatial patterns that were independent of one another (Rockhill et al., 2000).

Computational modeling

To evaluate further the hypothesis that anticlustering mechanisms account for cellular pattern formation in the inner retina of zebrafish, a computational model of cellular pattern formation during retinal growth was developed. This model attempted to mimic the geometry of life-long retinal growth in zebrafish, with cellular patterns formed across two-dimensional space from a band of precursor cells at the retinal margin (Fig. 1; see Materials

TABLE 2. Cross-Correlation Spatial Analysis Results for Cell-Type Pairs in the Inner Retina of Adult Zebrafish[1]

Cell type pair[2]	Nearest neighbor (μm; mean ± SD, n)	Conformity ratio[3] (mean/SD of NND)	Effective radius (μm; from cDRP)
PKC → Sub P	82.5 ± 46.1 (522)	1.8*	7.8
PKC → TH	32.2 ± 13.9 (63)	2.3*	12.6
5-HT → Sub P	75.3 ± 44.1 (46)	1.7*	18.3
	61.3 ± 27.5 (49)	2.2*	8.5
5-HT → TH	50.3 ± 22.5 (275)	2.2	17.9
Som → Sub P	57.7 ± 30.5 (16)	1.9*	18.4
	54.6 ± 24.4 (18)	2.2	23.7
Som → TH	47.6 ± 20.7 (25)	2.3*	19.6
	33.7 ± 16.9 (18)	2.0	10.1
	36.9 ± 17.8 (24)	2.1*	9.4
Sub P → PKC	12.1 ± 4.1 (12)	*3.0*	11.7
Sub P → 5-HT	29.9 ± 11.6 (10)	*2.6*	46.5
	28.4 ± 19.4 (10)	*1.5*	8.5
Sub P → Som	48.4 ± 19.2 (14)	*2.5*	18.4
	44.3 ± 20.1 (11)	*2.2*	23.7
TH → PKC	13.7 ± 1.6 (8)	n/a	12.6
TH → 5-HT	51.1 ± 36.8 (173)	1.4*	16.0
TH → Som	88.6 ± 48.4 (67)	1.8*	19.6
	43.5 ± 23.3 (29)	1.9*	10.1
	38.2 ± 16.3 (31)	2.3	9.4

[1]For abbreviations, see list.
[2]The "direction" of analysis (e.g., measuring NND from PKC-positive to substance P-positive cells) is indicated.
[3]Conformity ratio values denoted by an asterisk are not significantly different from those expected for uncorrelated patterns (at $P = 0.05$; Cook, 1996). Values in italics were interpreted as in Table 1.

and Methods). A relatively simple, lateral inhibition rule of cell fate acquisition was chosen for the initial modeling work. This inhibitory signal was released from all differentiated cells within the seed, and it inhibited precursor cells within the CGZ from acquiring the same fate as the seed cells (Fig. 2). Because the intrinsically low planimetric density limited the statistical significance of quantitative pattern analyses (Tables 1, 2), the patterns of substance P-positive cells were not utilized in the modeling work.

The initial modeling tests were aimed at determining whether model patterns could be generated with NND values that matched that of the corresponding seed. The results of these tests are presented in Figure 8, in which one of the free variables, λ_i or threshold, was varied as the other was held at a constant value. (All other model parameters were held constant across all simulations presented here.) For every seed pattern that was analyzed, values of λ_i and threshold were found for which the difference of the mean NND values for the seed and model patterns was estimated to be zero. When λ_i was represented as a normalized value relative to the NND of the individual data sets (i.e., λ_i/NND_{data}), and threshold was held constant at 1.0, no statistically significant differences were found between cell types, with the pooled values of (λ_i/NND_{data}) being 1.14 ± 0.09 (mean ± SD; Fig. 8A). When threshold was similarly analyzed with (λ_i/NND_{data}) held constant at 1.0, there was again no significant difference between cell types, with the pooled threshold values being 0.89 ± 0.24 (Fig. 8B).

These results indicated that for all of the analyzed cellular patterns, and across the different cell types, NND matches could be achieved between data and model patterns using a common set of threshold and (λ_i/NND_{data}) values. This cell-type–independent feature was based on the model's hypothesized anticlustering signaling mechanism, represented by λ_i, being spatially correlated with

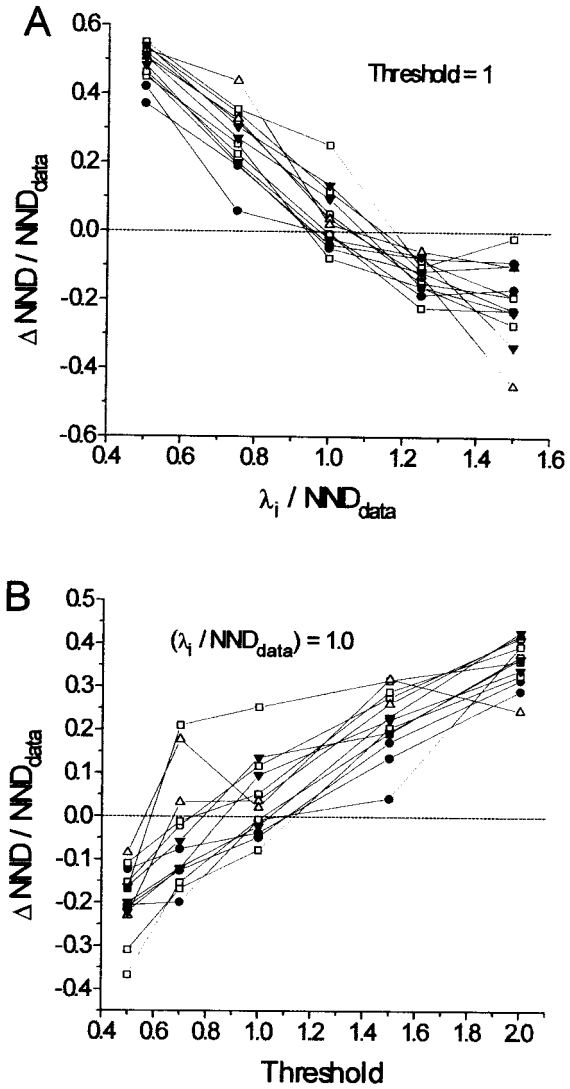

Fig. 8. Determination of optimal nearest neighbor distance (NND) matches between empirical and model cellular patterns. Either λ_i or threshold was varied (while the other was held constant), in an effort to determine whether the model could generate good matches between the data and model patterns, as defined by a difference between the respective mean NNDs (ΔNND) that was zero. Successful matches were determined for all the analyzed patterns, estimated by linear regression of each data file's ΔNND function. Note that in all cases, model patterns that were either too dense, or too sparse, could also be generated as a result of inappropriate values of λ_i and/or threshold. **A:** With threshold held at unity, a value of λ_i was inferred for each data file at which ΔNND was zero (to simplify graphical comparison across different data files and cell types, λ_i and ΔNND are plotted normalized to NND_{data}, the mean NND of the relevant seed). Across all cell types, the pooled values of (λ_i/NND_{data}) at which (ΔNND = 0) was 1.14 ± 0.09 (mean ± SD), with no statistical differences observed between cell types (independent Student's t-test). **B:** With (λ_i/NND_{data}) held at unity, a threshold was inferred for each data file as above. Across all cell types, the pooled values of threshold at which (ΔNND = 0) was 0.89 ± 0.24, estimated as above. For both panels: circles, PKC-positive cells; squares, TH-positive cells; upward triangles, somatostatin-positive cells; downward triangles, serotonin-positive cells.

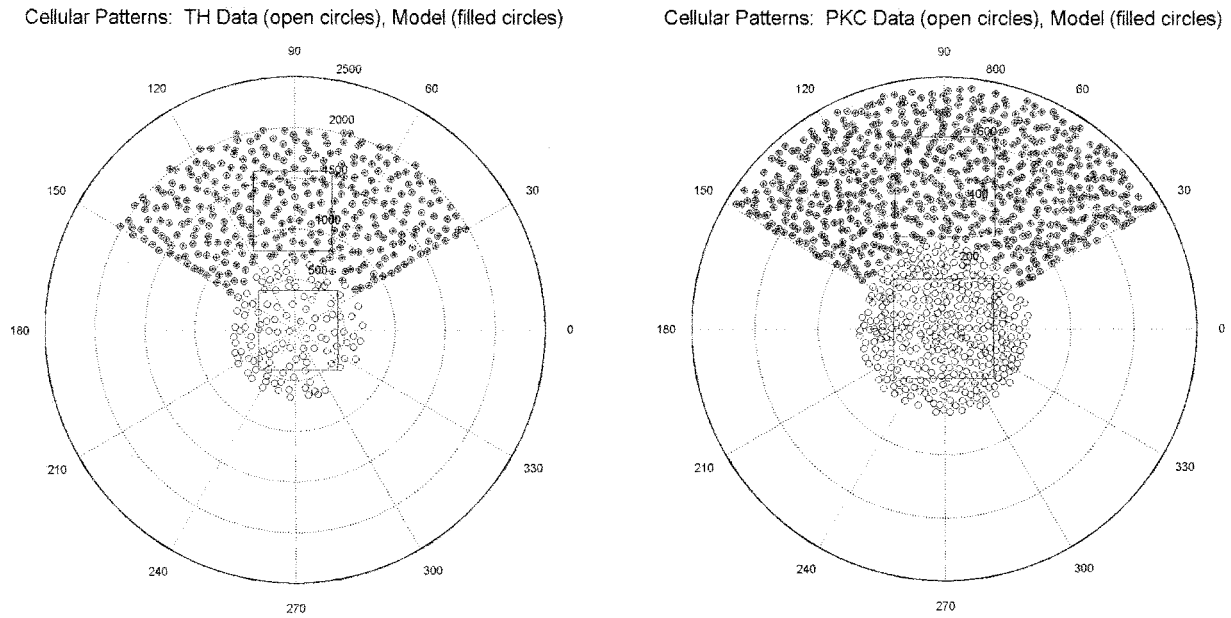

Fig. 9. Model cellular patterns for TH-positive (left) and PKC-positive cells (right) in adult zebrafish retina. For each simulation, threshold was set to 1.0, and (λ_i/NND_{data}) was set to 1.14 (see Results). In each panel the seed pattern of empirically derived cells is indicated by the open circles, and the model pattern is indicated by the filled circles (symbol sizes not to scale). The boxed regions within each pattern indicate those regions that were quantitatively analyzed (see Fig. 10). The numbers that increment radially from the center of the seed to the margin of the model pattern indicate the absolute distance in micrometers; note the different scales for the different cell types. Note the qualitative similarity between the data and model patterns for each cell type. For abbreviations, see list.

each cell type's local anticlustering pattern attribute, as represented by the NND distribution. Additionally, the values of λ_i were suggestive of a signaling mechanism that is either diffusible in nature or is delivered via cellular projections that extend beyond direct soma-to-soma contact (cf. the inferred λ_i values of Fig. 8A with the soma sizes evident from Cameron and Carney, 2000 and Fig. 6 of this report). Because of this implied generality in the signaling mechanism for pattern formation, for all subsequent modeling the values of threshold and (λ_i/NND_{data}) were held constant at 1.0 and 1.14, respectively.

The second tier of modeling experiments was aimed at determining whether these average, cell-type–independent signaling parameters produced model patterns with DRP and quadrat profiles that matched those of the empirical data, that is, determining whether local and long-range pattern characteristics of the model patterns matched those of the corresponding seeds. Two examples of cellular patterns generated by the model are illustrated in Figure 9, and the corresponding quantitative spatial analyses are presented in Figure 10. These results are representative of those derived for the other cell types. Visual inspection of the seeds and their corresponding model patterns reveal similarities in patterning (Fig. 9). The qualitative similarities were supported by the quantitative spatial analyses. Specifically, for each seed that was analyzed, the derived model pattern had similar spatial characteristics, as judged by the NND, quadrat, and DRP analyses. Two examples are illustrated in Figure 10. Expressed as a percentage and pooled across all analyzed data files (n = 13), the mean NND values for the seed and model patterns differed by 0.11 ± 7.2% of the empirical NND, and the effective radius values differed by −7.3 ± 23.1% of the empirical effective radius values. Quadrat analysis revealed that all the model patterns had profiles that were similar to the corresponding seed (either regular, or neither regular nor aggregated, as in Fig. 7). No post-differentiation manipulations of cellular patterns, such as tangential cellular movements, were required in the model to attain good matches between the seed and the model patterns. These results indicated that the hypothesized signaling mechanism, which controls the spatiotemporal profile of cell fate decisions during retinal growth, could generate model cellular patterns that closely matched those of the empirically observed patterns, as judged by three different spatial pattern-analysis techniques.

DISCUSSION

The results of this study suggest that cellular patterns in the inner retina of adult zebrafish—and their formation during retinal growth—are characterized by general organizational principles. First, the somata of a given cell type are arrayed within two-dimensional patterns that are characterized by anticlustering. Second, for most cell types there is little evidence for long-range, nonrandom pattern features. Third, the patterns of different cell types are often independent of one another. The generality of these results motivated the development of a computational model of cellular pattern formation in the zebrafish retina, which in turn suggested that a relatively simple signaling scheme—modeled as a spatiotemporal regulation of cell fate decisions—could account for all the observed cellular patterns. These principles, and hypothesized mechanisms of cellular pattern formation, are discussed below.

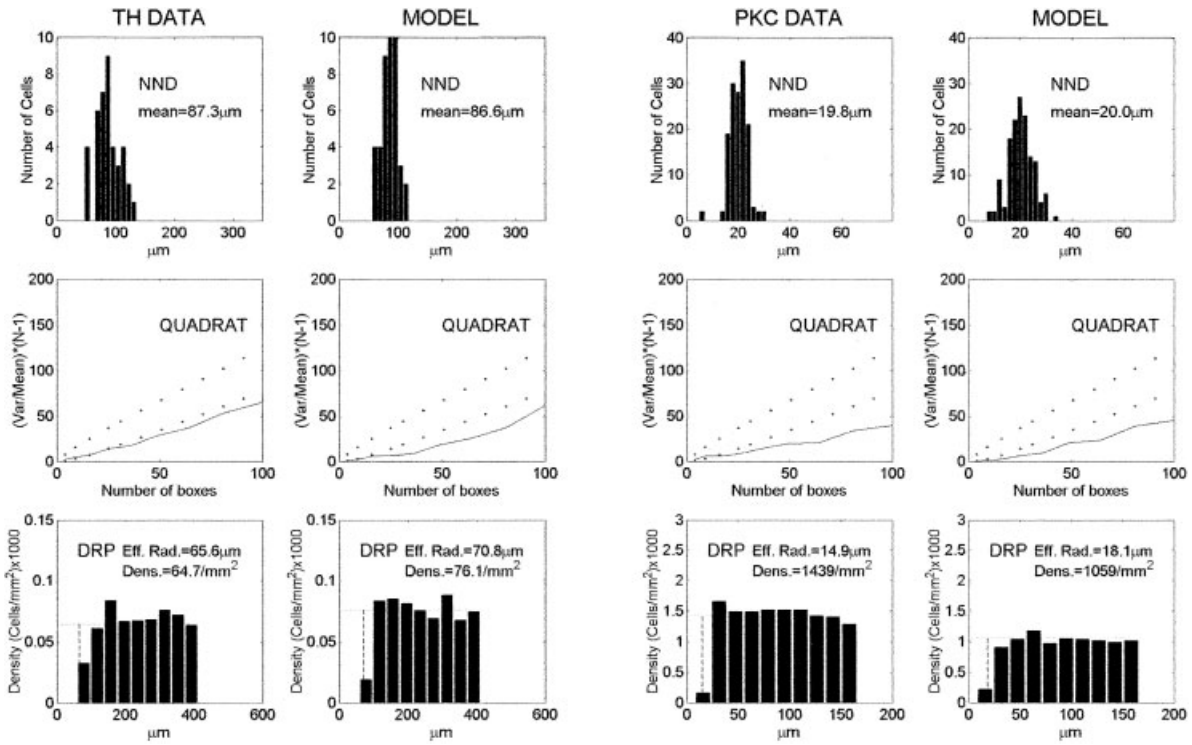

Fig. 10. Quantitative spatial analysis results for the data and model patterns illustrated in Figure 9. **Left (top to bottom):** NND, quadrat, and DRP analyses for the seed and model patterns of TH-positive cells. Note the similarity between the data and model patterns: similar means (and distributions) of the NND; similar quadrat analysis functions (cf. Fig. 7); similar effective radius values and anticlustering phenomena indicated by the DRP analysis. **Right (top to bottom):** NND, quadrat, and DRP analyses for the seed and model patterns of PKC-positive cells. The data and model patterns of PKC-positive cells had similar characteristics, as objectively determined by the quantitative spatial analyses. For abbreviations, see list.

Anticlustering of cellular patterns

Each analyzed cell type was arrayed in a pattern characterized by anticlustering, that is, each soma of a given cell type was surrounded by a two-dimensional area that was devoid of homotypic somata. Because the size of these exclusion zones is significantly larger than the dimensions of individual somata (Cameron and Carney, 2000), it is possible that the anticlustering phenomena could arise from signaling mechanisms that operate beyond the spatial extent enabled by direct soma-to-soma contact. At the molecular level such mechanisms could include diffusible agents or intercellular contacts via cellular projections such as dendrites. Diffusible signaling mechanisms have previously been implicated in ocular development, including mechanisms that involve ligands of the epidermal growth factor receptor (e.g., Baonza et al., 2001), ligands of the retinoic acid receptor (for review, see Adler, 1993), and the *hedgehog* signaling system (Stenkamp et al., 2000; Neumann and Nuesslein-Volhard, 2000). Additionally, dendrodendritic interactions have previously been suggested as a mechanism for regulating cellular pattern formation in the vertebrate retina (Galli-Resta, 2000; Eglen et al., 2000), and a testable hypothesis for future studies is that the λ_i values derived from the current model are correlated with the spatial characteristics of the corresponding cell type's dendritic arbor. The results of the current study cannot rule out the operation of direct soma-to-soma signaling mechanisms during pattern formation of the inner nuclear layer in zebrafish. The results do suggest, however, that molecular signaling schemes that extend spatially beyond soma-to-soma contact could be important mechanisms of cellular pattern formation in the inner retina of zebrafish.

Cellular patterns are neither regular nor aggregated over large spatial scales

Most of our evidence, derived from quadrat analysis, suggested that the patterns of inner retinal cells are not statistically different from random patterns over large spatial scales (which is not to say that the patterns are indeed random). This observation is in contrast to the regular patterns of cone photoreceptors that are commonly observed in teleosts (e.g., Stenkamp et al., 2001), including zebrafish (Larison and BreMiller, 1990; Robinson et al., 1993). The lack of pattern regularity over large spatial scales cannot rule out the operation of long-range spatial organizing mechanisms during retinal development and growth, but it does suggest that cellular pattern formation in the inner nuclear layer of zebrafish is dominated by signaling mechanisms that operate over relatively short spatial distances. In terms of functional considerations for an individual cell, the lack of nonrandom patterns over large spatial extents suggests that the precise spatial location of a homotypic soma beyond some critical distance (e.g., two or three mean nearest neighbor distances) may not be significant.

A consistent exception to the general rule of long-range "randomness" was observed. PKC-positive bipolar cells were arrayed in patterns that were always regular over large distances. It is unclear whether a functional or developmental significance can be attached to the spatial regularity of this cell type, which receives considerable synaptic input from rod photoreceptors (Suzuki and Kaneko, 1990). It may be that some second-order neurons in the zebrafish retina are arrayed in regular patterns in order to achieve an isotropic sampling of photoreceptor inputs. The modeling results of this report do indicate that both regular and nonregular patterns can arise from the same, relatively simple rule of homotypic inhibition of cell fate decisions during retinal growth (see below).

Independence of cellular patterns

Although the analyzed cellular patterns in this study share an anticlustering characteristic, their two-dimensional patterns were generally independent of one another (Table 2), similar to observations made previously for the inner retina of rabbit (Rockhill et al., 2000). This result indicates that the mechanisms controlling cellular pattern formation in the inner nuclear layer are, at some level, necessarily different between different cell types. If each cell type had utilized a common spatial organizing mechanism, the patterns should have been positively correlated, even if they differed in density. It is unclear, however, how selective signaling can be achieved in this system. Although instructive patterning cues between cells of different types have been suggested in the outer retina (Stenkamp et al., 1996), the independence between cellular patterns, and the model's ability to produce cellular patterns using a signaling scheme that is cell-type specific, argue that instructive cues between different cell types may not be a universal component of cellular pattern formation in the inner retina.

With respect to neurophysiological processing, independence between cellular patterns may not be surprising: if dendritic arbors are the structural foundation of neural processing, spatial registration between the somata of different cell types may be of comparatively minimal consequence. One hypothesis is that the nonrandom patterns are "echoes" of developmental events, with such patterns having originally served as templates for the spatial establishment and alignment of pre- and postsynaptic structures. Perhaps by regulating cellular pattern formation at, or near, the spatiotemporal point of cell fate decision—and by minimizing instructive interactions between heterotypic cells—the retina can achieve its proper, two-dimensional organization at relatively minimal metabolic cost. On this general point the results of Kouyama and Marshak (1997) are noteworthy, as they indicate a positive spatial correlation between short-wavelength–sensitive cone photoreceptors and their synaptically associated bipolar cells in the primate retina. It remains possible, therefore, that future investigations might reveal inner retinal cell types in the zebrafish that are arrayed in patterns that are positively correlated: it is already known that the different spectral classes of cone photoreceptors in the zebrafish retina are so organized (e.g., Robinson et al., 1993).

Mechanisms for regulating cellular pattern formation in the inner retina of zebrafish: a hypothesized "one-step" mechanism

Cellular pattern formation in the vertebrate central nervous system is an extremely complex phenomenon. A first-order geometric requirement for proper functionality is that millions of cells, comprising hundreds of different cell types, must be properly arrayed within three-dimensional space. At the current time no single model accounts for the mechanisms that control the assembly of such a complex structure. However, computational techniques can be successfully applied to restricted aspects of cellular pattern formation—such as how nonrandom, two-dimensional patterns of cells can arise from an undifferentiated neuroepithelium—and from these studies insights regarding the molecular mechanisms that regulate cellular pattern formation can be developed and ultimately tested.

In the current study, a computational modeling approach was used to determine whether a relatively simple, physically realistic signaling scheme could account for aspects of cellular pattern formation and structure in the zebrafish inner retina. In this "proof of principle" model, cellular patterns very similar to those observed empirically arose via the operation of a signal, arising from differentiated cells, that inhibits the generation of the homotypic cell type. This type of inhibitory signaling mechanism, arising from differentiated retinal cells, has previously been implicated in the genesis of specific cell types during vertebrate retinal development, including TH-positive cells (Negishi et al., 1982; Reh and Tully, 1986), amacrine cells (Belliveau and Cepko, 1999), and ganglion cells (Waid and McLoon, 1998).

This inhibitory signaling mechanism successfully accounted for all the objective, quantitative aspects of cellular patterns, including anticlustering. We note that the zebrafish retina is a popular system for investigating the signaling mechanisms that control retinal development (e.g., Fadool et al., 1997; Malicki and Driever, 1999; Doerre and Malicki, 2001; Jensen et al., 2001; Kay et al., 2001), and mechanistic roles for cell-surface (Link et al., 2000; Scheer et al., 2001) and diffusible agents (Hyatt et al., 1996; Stenkamp et al., 2000; Neumann and Nuesslein-Volhard, 2000) have been reported. Our model thus seems consistent with physically realistic signaling mechanisms that are known to regulate zebrafish retinal development.

A key feature of our model's prediction is that the growing retina utilizes signaling mechanism(s) that directly affect cellular pattern formation at, or near, the spatiotemporal point of cell fate decision. No tangential migrations of differentiated cells were necessary in the current model to provide reasonable matches to the empirical cell patterns (however, see Eglen and Willshaw, 2002). In many neural structures such migrations are critical for the proper establishment of cellular patterns, with a classic example being the migration of differentiated neurons during cerebellar development (for review, see Goldowitz and Hamre, 1998). Tangential movements of differentiated somata have also been reported in vertebrate retinas (Hendrickson, 1994; Reese et al., 1995, 1999; Galli-Resta et al., 1997; Galli-Resta, 2000), and computational models of cellular pattern formation in other model retinal systems support the importance of such mechanisms (Eglen et al., 2000; Eglen and Willshaw, 2002). The current study

does not rule out a role for tangential movements of differentiated somata during zebrafish retinal development, and indeed this mechanism could formally provide the "one-step" mechanism inferred by the modeling results. The overall effectiveness and general applicability of the current model's control of cell fate decisions, however, suggests that for many neuronal cell types within the inner nuclear layer of zebrafish, cellular pattern formation might be dominated by signaling mechanisms that establish the two-dimensional patterns at, or very near to, the spatiotemporal point of cell fate decision.

ACKNOWLEDGMENTS

We thank Dr. Eduardo Solessio for helpful comments regarding the article.

LITERATURE CITED

Adler R. 1993. Determination of cellular fates in the retina. Invest Ophthalmol Vis Sci 34:1677–1682.

Ali MA, Anctil M. 1976. Retinas of fishes: an atlas. Berlin: Springer-Verlag.

Baonza A, Casci T, Freeman M. 2001. A primary role for the epidermal growth factor receptor in ommatidial spacing in the *Drosophila* eye. Curr Opin Cell Biol 11:396–404.

Belliveau MJ, Cepko CL. 1999. Extrinsic and intrinsic factors control the genesis of amacrine and cone cells in the rat retina. Development 126:555–566.

Bonini NM, Choi KW. 1995. Early decisions in *Drosophila* eye morphogenesis. Curr Opin Gen Dev 5:507–515.

Cameron DA. 1995. Asymmetric retinal growth in the adult teleost green sunfish (*Lepomis cyanellus*). Vis Neurosci 12:95–102.

Cameron DA, Carney LH. 2000. Cell mosaic patterns in the native and regenerated inner retina of zebrafish: implications for retinal assembly. J Comp Neurol 430:356–367.

Cameron DA, Easter SS, Jr. 1993. The cone photoreceptor mosaic of the green sunfish, *Lepomis cyanellus*. Vis Neurosci 10:375–384.

Cook JE. 1996. Spatial properties of retinal mosaics: an empirical evaluation of some existing measures. Vis Neurosci 13:15–30.

Cook JE, Chalupa LM. 2000. Retinal mosaics: new insights into an old concept. Trends Neurosci 23:26–34.

David FN, Moore PG. 1954. Notes on contagious distributions in plant populations. Ann Bot (Lond) 18:47–53.

Diaz-Araya C, Provis JM. 1992. Evidence of photoreceptor migration during early foveal development: a quantitative analysis of human fetal retinae. Vis Neurosci 8:505–514.

Doerre G, Malicki J. 2001. A mutation of early photoreceptor development, *mikre oko*, reveals cell-cell interactions involved in the survival and differentiation of zebrafish photoreceptors. J Neurosci 21:6745–6757.

Dowling JE. 1987. The retina. Cambridge: Belknap.

Eglen SJ, Willshaw DJ. 2002. Influence of cell fate mechanisms upon retinal mosaic formation: a modeling study. Development 129:5399–5408.

Eglen SJ, van Ooyen A, Willshaw DJ. 2000. Lateral cell movement driven by dendritic interactions is sufficient to form retinal mosaics. Network 11:103–118.

Engström K. 1963. Cone types and cone arrangements in teleost retinae. Acta Zool 44:179–243.

Fadool JM, Brockerhoff SE, Hyatt GA, Dowling JE. 1997. Mutations affecting eye morphology in the developing zebrafish (*Danio rerio*). Dev Genet 20:288–295.

Galli-Resta L. 1998. Patterning the vertebrate retina: the early appearance of retinal mosaics. Semin Cell Dev Biol 9:279–284.

Galli-Resta L. 2000. Local, possible contact-mediated signaling restricted to homotypic neurons controls the regular spacing of cells within the cholinergic arrays in the developing rodent retina. Development 127:1509–1516.

Galli-Resta L, Resta G, Tan SS, Reese BE. 1997. Mosaics of Islet-1-expressing amacrine cells assembled by short-range cellular interactions. J Neurosci 17:7831–7838.

Goldowitz D, Hamre K. 1998. The cells and molecules that make a cerebellum. Trends Neurosci 21:375–382.

Grieg-Smith P. 1964. Quantitative plant ecology. London: Butterworths.

Hannover A. 1840. Ueber die Netzhaut und ihre Gehirnsubstanz bei Wirbelthieren, mit Ausnahme des Menschen. Archic fur Anatomie, Physiologie und Wissenschaftliche Medicin 320–345.

Hendrickson AE. 1994. Primate foveal development: a microcosm of current questions in neurobiology. Invest Ophthalmol Vis Sci 35:3129–3133.

Hibbard E. 1971. Grid patterns in the retinal organization of the cichlid fish *Astronotus ocellatus*. Exp Eye Res 12:175–180.

Hyatt GA, Schmitt EA, Fadool JM, Dowling JE. 1996. Retinoic acid alters photoreceptor development in vivo. Proc Natl Acad Sci U S A 93:13298–13303.

Jensen AM, Walker C, Westerfield M. 2001. *mosaic eyes*: a zebrafish gene required in pigmented epithelium for apical localization of retinal cell division and lamination. Development 128:95–105.

Kay JN, Finger-Baier KC, Roeser T, Staub W, Baier H. 2001. Retinal ganglion cell genesis requires *lakritz*, a Zebrafish *atonal* homolog. Neuron 30:725–736.

Kopan R, Cagan R. 1997. Notch on the cutting edge. Trends Genet 13:465–467.

Kouyama N, Marshak DW. 1997. The topographical relationship between two neuronal mosaics in the short wavelength-sensitive system of the primate retina. Vis Neurosci 14:159–167.

Larison KD, BreMiller R. 1990. Early onset of phenotype and cell patterning in the embryonic zebrafish retina. Development 109:567–576.

Link BA, Fadool JM, Malicki J, Dowling JE. 2000. The zebrafish young mutation acts noncell-autonomously to uncouple differentiation from specification for all retinal cells. Development 127:2177–2188.

Malicki J, Driever W. 1999. *oko meduzy* mutations affect neuronal patterning in the zebrafish retina and reveal cell-cell interactions of the retinal neuroepithelial sheet. Development 126:1235–1246.

Marshak DW, Yamada T, Stell WK. 1984. Synaptic contacts of somatostatin-immunoreactive amacrine cells in the goldfish retina. J Comp Neurol 225:44–52.

Müller H. 1857. Anatomisch-physiologische Untersuchungen üer die Retina des Menschen und der Wirbeltiere. Z Wiss Zool 8:1–122.

Negishi K, Teranishi T, Kato S. 1982. New dopaminergic and indoleamine-accumulating cells in the growth zone of goldfish retina after neurotoxic destruction. Science 216:747–749.

Neumann CJ, Nuesslein-Volhard C. 2000. Patterning of the zebrafish retina by a wave of sonic hedgehog activity. Science 289:2137–2139.

Podugolnikova TA. 1985. Morphology of bipolar cells and their participation in spatial organization of the inner plexiform layer of jack mackerel retina. Vision Res 25:1843–1851.

Polyak SL. 1941. The vertebrate visual system. Chicago: University of Chicago Press.

Powers MK, Raymond, PA. 1990. Development of the visual system. In: Douglas, RH, Djamgoz MBA, editors. The visual system of fish. London: Chapman and Hall. p 419–442.

Ramón y Cajal S. 1893. La rétine des vertébrés. Cellule 9:17–257.

Reese BE, Galli-Resta L. 2002. The role of tangential dispersion in retinal mosaic formation. Prog Retin Eye Res 21:153–168.

Reese BE, Harvey AR, Tan S-S. 1995. Radial and tangential dispersion patterns in the mouse retina are cell-class specific. Proc Natl Acad Sci U S A 92:2494–2498.

Reese BE, Necessary BD, Tam PP, Faulkner-Jones B, Tan S-S. 1999. Clonal expansion and cell dispersion in the developing mouse retina. Eur J Neurosci 11:2965–2978.

Reh TA, Tully TT. 1986. Regulation of tyrosine hydroxylase-containing amacrine cell number in larval frog retina. Dev Biol 114:463–469.

Ripley BD. 1981. Spatial statistics. New York: John Wiley & Sons.

Robinson J, Schmitt EA, Harosi FI, Reece RJ, Dowling JE. 1993. Zebrafish ultraviolet visual pigment: absorption spectrum, sequence, and localization. Proc Natl Acad Sci U S A 90:6009–6012.

Robinson SR, Hendrickson AE. 1995. Shifting relationships between photoreceptors and pigment epithelial cells in monkey retina: implications for the development of retinal topography. Vis Neurosci 12:767–778.

Rockhill RL, Euler T, Masland RH. 2000. Spatial order within but not between types of retinal neurons. Proc Natl Acad Sci U S A 97:2303–2307.

Rodieck RW. 1991. The density recovery profile: a method for the analysis

of points in the plane applicable to retinal studies. Vis Neurosci 6:95–111.

Scheer N, Groth A, Hans S, Campos-Ortega JA. 2001. An instructive function for Notch in promoting gliogenesis in the zebrafish retina. Development 128:1099–1107.

Stenkamp DL, Cameron DA. 2002. Cellular pattern formation in the retina: retinal regeneration as a model system. Mol Vision 8:280–293.

Stenkamp DL, Hisatomi O, Barthel LK, Tokunaga F, Raymond PA. 1996. Temporal expression of rod and cone opsins in embryonic goldfish retina predicts the spatial organization of the cone mosaic. Invest Ophthalmol Vis Sci 37:363–376.

Stenkamp DL, Frey RA, Prabhudesai SN, Raymond PA. 2000. Function for Hedgehog genes in zebrafish retinal development. Dev Biol 220:238–252.

Stenkamp DL, Powers MK, Carney LH, Cameron DA. 2001. Evidence for two distinct mechanisms of neurogenesis and cellular pattern formation in regenerating goldfish retinas. J Comp Neurol 431:363–381.

Strigini M, Cohen SM. 1999. Formation of morphogen gradients in the *Drosophila* wing. Semin Cell Dev Biol 10:335–344.

Suzuki S, Kaneko A. 1990. Identification of bipolar cell types by protein kinase C-like immunoreactivity in the goldfish retina. Vis Neurosci 5:223–230.

Takesue A, Mochizuki A, Iwasa Y. 1998. Cell-differentiation rules that generate regular mosaic patterns: modelling motivated by cone mosaic formation in fish retina. J Theor Biol 194:575–586.

Tohya S, Mochizuki A, Iwasa Y. 1999. Formation of cone mosaic of zebrafish retina. J Theor Biol 200:231–244.

Vincent JP, Dubois L. 2002. Morphogen transport along epithelia, an integrated trafficking problem. Dev Cell 3:615–623.

Waid DK, McLoon SC. 1998. Ganglion cells influence the fate of dividing retinal cells in culture. Development 125:1059–1066.

Wässle H, Riemann HJ. 1978. The mosaic of nerve cells in the mammalian retina. Proc R Soc Lond B 200:441–461.

Wikler KC, Rakic P. 1990. Distribution of photoreceptor subtypes in the retina of diurnal and nocturnal primates. J Neurosci 10:3390–3401.

Williams DR. 1988. Topography of the foveal cone mosaic in the living human eye. Vision Res 28:433–454.

Yazulla S, Zucker CL. 1988. Synaptic organization of dopaminergic interplexiform cells in the goldfish retina. Vis Neurosci 1:13–29.

Yazulla S, Studholme KM, Zucker CL. 1985. Synaptic organization of substance P-like immunoreactive amacrine cells in goldfish retina. J Comp Neurol 231:232–238.

Zipursky SL, Rubin GM. 1994. Determination of neuronal cell fate: lessons from the R7 neuron of *Drosophila*. Annu Rev Neurosci 17:373–397.